Multi-link MIMO channel modeling using geometry-based approach

Poutanen, Juho; Tufvesson, Fredrik; Haneda, Katsuyuki; Kolmonen, Veli-Matti; Vainikainen, Pertti

Published in:
IEEE Transactions on Antennas and Propagation

DOI:
10.1109/TAP.2011.2122296

2012

Multi-Link MIMO Channel Modeling Using Geometry-Based Approach

Juho Poutanen, Fredrik Tufvesson, *Senior Member, IEEE*,
Katsuyuki Haneda, *Member, IEEE*, Veli-Matti Kolmonen, and Pertti Vainikainen

***Abstract*—This paper presents an approach to extend geometry-based stochastic channel models (GSCMs) to support multi-link simulations by applying the concept of common clusters. The idea of the proposed approach is to control the correlation between different links, inter-link correlation, by adjusting the amount of power simultaneously propagating via the same clusters in the different links. A multi-link GSCM is proposed, and the effects that the common clusters have on inter-link correlation and on sum rate capacity are investigated based on simulations. In addition, the behavior of common clusters is analyzed based on dual-link channel measurements. Finally, comparison between simulations and measurements is done in order to indicate the validity of the proposed multi-link GSCM.**

***Index Terms*—Radio channel modeling, geometry-based channel modeling, multi-link channel modeling, multi user MIMO.**

I. Introduction

GEOMETRY- based stochastic channel models (GSCMs) have attained much attention in MIMO channel modeling during the past decade. This is due to their inherent capability of modeling spatial and temporal correlation properties in a straightforward manner. The basic idea behind the GSCMs is to emulate the double-directional radio channel by placing clusters in the simulation environment to act as physical scattering objects. The clusters consist of groups of closely located multipath propagation components (MPCs), and the directions, delays, and complex amplitudes of each MPC are directly computed based on the geometry of the simulation environment. Examples of GSCMs, which all rely on the cluster approach, are the COST 259 [1], COST 273 [2], and WINNER [3] channel models.

A. Motivation

Even though the state-of-the art GSCMs are extremely sophisticated, the capability of the current implementations to simulate multi-link scenarios has up to now remained an open question. In principle, the cluster-based structure of the GSCMs supports multi-link simulations just by dropping multiple mobile stations (MSs) and/or base stations (BSs) into the environment. However, the major open question has so far been how to control the correlation between different links, the inter-link correlation. Since clusters are generated randomly and independently for each link, there is no guarantee that the different links result in having proper correlation with respect to each other. Based on previously reported works, however, it has been realized that different links may encounter remarkable inter-link correlation when the units are in close proximity to each other [4] and even if they would be largely separated in distance [5] – [8]. Two links may also have very different inter-link correlation even if they are in the same environment (e.g. in the same room) [9].

Those experimental findings indicate a true need for multi-link MIMO channel models being able to reflect those properties. Furthermore, since the trend in novel radio communication systems is going more and more towards applications that utilize links between multiple nodes in the network in their operation, the need for realistic multi-link channel model increases accordingly. Examples of such systems where it would be very beneficial to have realistic multi-link channel models include cooperative communication systems, and indoor localization applications. Underestimating or neglecting the inter-link correlation would usually lead to too optimistic performance results in system simulations [4].

To the authors' best knowledge, previous works on multi-link MIMO channel modeling are restricted to the analytical dual-link model proposed in [10]; no contributions on multi-link GSCMs are available in the open literature.

B. Contributions

In this paper we propose an approach for extending a general GSCM to fully support multi-link simulations by applying the concept of *common clusters* (CCs). In short, the idea behind the proposed method is to control the correlation between different links by allowing a certain proportion of the energy in different links to propagate through the same clusters. The concept of CCs was first introduced in [6], where it was also shown based on measurements that significant amounts of energy can indeed propagate through the same scatterers in different MIMO links in certain types of environments.

This paper has been written within the framework of WILATI+ which is a joint project between three Scandinavian universities and a part of the NORDITE research program funded by the Finnish, Swedish and Norwegian national research institutes Tekes, Vinnova and RCN, respectively. The work has been partly funded also by the Jenny and Antti Wihuri Foundation and the post-doctoral research project of the Academy of Finland, Helsinki, Finland.

Juho Poutanen, Katsuyuki Haneda, Veli-Matti Kolmonen, and Pertti Vainikainen are with the Department of Radio Science and Engineering, Aalto University School of Science and Technology, Finland.

Fredrik Tufvesson is with the Department of Electrical and Information Technology, Lund University, Sweden.

At first, a simple multi-link GSCM is implemented based on the concept of CCs. The developed model is used to study the effect of the CCs on channel characteristics and system performance from two perspectives: first, it is shown that CCs are a suitable way of adjusting the correlation between different links, and, second, the effect of the CCs on channel capacity is investigated. In the later part of the paper, CCs are analyzed based on measured dual-link MIMO data. It is also shown that the developed multi-link GSCM is able to accurately predict the channel behavior in comparison with the measurement data. Even though the GSCM developed in this paper is rather simple, the modeling concepts are fully applicable to more sophisticated GSCM implementations (such as [1] – [3]), as well and it should be straightforward to extend those models to handle the multi-link scenario.

C. Organization

The remainder of the paper is organized as follows. In Section II, the modeling philosophy of the multi-link GSCMs is discussed, followed by a detailed description of the model developed in this work. Section III is dedicated for the simulation analyses of the effect of the CCs on inter-link correlation and dual-link capacity. In Section IV, CCs are extracted from dual-link channel measurement data. In addition, the developed GSCM is compared with the measurement data in terms of the dual-link channel capacity in Section IV. Finally, Section V concludes the work.

II. Multi-Link Geometry-Based Channel Modeling

When extending the current GSCMs to cover multi-link scenarios there are two main aspects to consider: 1) The singe-link behavior should remain the same, while at the same time 2) the correlation between links, i.e. interlink correlation, should be represented in a realistic way.

In this section, a concept for extending the current GSCMs to support multi-link simulations is presented. First, the concept of common clusters, the proposed methodology in which the correlation between links in GSCMs can be controlled, is explained. Then, the implementation of the multi-link GSCM used in this paper is detailed.

A. Concept of common clusters (CCs)

A common cluster is a cluster that contributes to the channel between *different* links at the same time, as shown in Fig. 1. Since the amount of power carried by the CCs can be set to a desired value, it is possible to control the inter-link correlation between different links; the larger is the amount of power that is propagating via the CCs, the stronger is the correlation between the different links. The intra-link correlation, i.e. the correlation between antenna elements in a MIMO link, is as before controlled by the cluster distributions and remains unchanged. The approach is based on [6], where the concept of the CC was first introduced. There measurement results also showed that CCs can carry significant parts of the energy in realistic multi-link environments.

B. Multi-link GSCM development

In the proposed multi-link GSCM, clusters are generated so that each link is assigned with a set of *uncommon clusters* (UCCs) and a certain number of CCs. The UCCs are generated separately for each link and they contribute only to the impulse response of the designated link, whereas CCs are shared by the different links and contribute to both transfer functions (or impulse responses), see Fig. 1. In order to control the correlation between different links, the amount of power that propagates through the CC is set to a desired value by the following procedure. First, the propagation path parameters, including the directions of departure (DoD) and –arrival (DoA), delay, and complex amplitude, are calculated for each MPC according to the geometrical locations of the antennas and clusters. Then, the power carried by the UCCs is scaled with a factor of L so that the condition

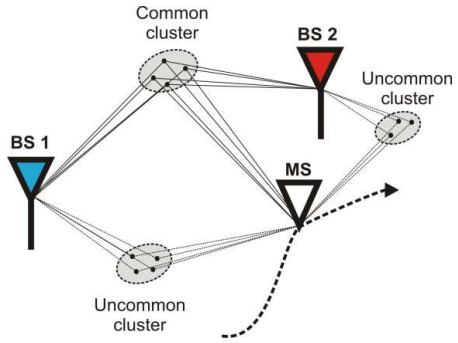

Fig. 1. Example of a common cluster (CC) in a scenario with one MS and two BSs. The correlation between different links can be controlled by changing the amount of power that propagates through the CC.

$$S_{\text{common}} = \frac{P_{\text{CC}}}{L \cdot P_{\text{UCC}} + P_{\text{CC}}} \tag{4}$$

is satisfied. In (4), S_{common} is a measure called *the significance of common cluster*, which defines the ratio between powers carried by the CCs and UCCs; P_{CC} and P_{UCC} are the sum of powers carried by all the CCs and UCCs, respectively.

Once the propagation path parameters with the desired S_{common} have been obtained, the MIMO channel matrices are calculated for each link in the same way as for a conventional GSCM as

$$\mathbf{H} = \sum_{p=1}^{P} \alpha_p \, \boldsymbol{a}_p^{\text{RX}} (\boldsymbol{a}_p^{\text{TX}})^T e^{j(2\pi f \tau_p + \xi(p))} \in \mathbb{C}^{N_r \times N_t}, \tag{5}$$

where P is the number of MPCs, α_p is the amplitude of the p-th MPC, f is the used radio frequency, τ_p is the propagation delay of the p-th MPC, and $(\cdot)^T$ denotes the matrix transpose operation. Furthermore, $\boldsymbol{a}_p^{\text{TX}}$ and $\boldsymbol{a}_p^{\text{RX}}$ are the array response vectors calculated at the transmitter (TX) or receiver (RX) as

$$\boldsymbol{a}_p^{\text{TX,RX}} = \left[\exp\left(\mathrm{j}k\langle \boldsymbol{r}_1 \boldsymbol{u}_p \rangle\right) \cdots \exp\left(\mathrm{j}k\langle \boldsymbol{r}_N \boldsymbol{u}_p \rangle\right)\right] \tag{6}$$

where $k = \frac{2\pi}{\lambda}$ is the wave number, $\boldsymbol{u}_p$ is the unit directional vector consisting of the DoD and DoA of the p-th MPC, and $\boldsymbol{r}_n$ is the position vector of the n-th antenna element in the array. The term $\langle \boldsymbol{r}_N \boldsymbol{u}_p \rangle$ represents the inner product between vectors $\boldsymbol{r}_N$ and $\boldsymbol{u}_p$. Finally, a random phase $\xi(p)$ is added to each MPC in order to increase the number of independent realizations of the channel matrices [11].

III. Inter-Link Correlation and Dual-Link MIMO Channel Capacity

In this section, the effect of the common clusters, or more precisely S_{common}, on system characteristics is studied in terms of 1) the inter-link correlation and 2) the sum rate dual-link MIMO capacity when using the multi-link GSCM described in Section II. After defining the inter-link correlation and sum rate dual-link MIMO capacity, we evaluate them in different environments. In the following, the analysis is restricted to a dual-link scenario with one TX and two RXs.

A. Definitions

1) Inter-link correlation

The inter-link correlation was evaluated by calculating the correlation matrix collinearity (*CMC*, or "collinearity") as [12]

$$CMC = \frac{\left|\text{tr}\{\mathbf{R}_1\mathbf{R}_2^{\text{H}}\}\right|}{\|\mathbf{R}_1\|_{\text{F}}\|\mathbf{R}_2\|_{\text{F}}}, \tag{7}$$

where $\mathbf{R}_i$ is the correlation matrix of the *i*-th link calculated as

$$\mathbf{R}_i = \frac{\sum_{s=1}^{N_s}\left(\mathbf{H}(s)^{(i)}\right)^{\text{H}}\mathbf{H}(s)^{(i)}}{\frac{1}{N_t}\sum_{s=1}^{N_s}\|\mathbf{H}(s)^{(i)}\|_{\text{F}}^2}. \tag{8}$$

In equations (7) and (8), $(\cdot)^{\text{H}}$ is the complex transpose of a matrix; N_s is the number of independent channel realizations; N_t is the number of transmit antennas; and $\|\cdot\|_{\text{F}}$ denotes the Frobenius norm.

The *CMC* describes how similar the subspaces of the correlation matrices of the different links are, ranging between zero (matrices are orthogonal to each other) and one (matrices are similar).

2) Sum rate dual-link capacity

The capacity values were calculated in the following way. First, the received power for the *i*-th link P_i was calculated as

$$P_i = \frac{1}{N_s \cdot N_r \cdot N_t}\sum_{s=1}^{N_s}\|\mathbf{H}_i(s)\|_{\text{F}}^2, \tag{9}$$

where N_s is the number of independent channel realizations; N_r is the number of receive antennas; N_t is the number of transmit antennas; $\mathbf{H}_i$ is the channel matrix of the *i*-th link; and $\|\cdot\|_{\text{F}}$ denotes the Frobenius norm. In order to calculate the capacity, the channel matrices were normalized as

$$\widehat{\mathbf{H}}_i(s) = \frac{\mathbf{H}_i(s)}{\sqrt{P_i}}. \tag{10}$$

In the dual-link case, the received signal can be written as [13]

$$\mathbf{y} = \sqrt{\rho}\widehat{\mathbf{H}}_1\mathbf{x}_1 + \sqrt{\eta}\widehat{\mathbf{H}}_2\mathbf{x}_2 + \mathbf{n}, \tag{11}$$

where $\widehat{\mathbf{H}}_1$ and $\widehat{\mathbf{H}}_2$ are the normalized channel matrices of the desired and interfering link. The ρ and η are the signal-to-noise ratio (SNR) and interference-to-noise ratio (INR), respectively, $\mathbf{x}_1$ and $\mathbf{x}_2$ are the transmitted signal vectors, and and $\mathbf{n}$ is a noise vector. The capacity values were calculated for each channel realization as [13]

$$C(\widehat{\mathbf{H}}_1) = \log_2\left[\det\left(\mathbf{I}_{N_r} + \frac{\rho}{N_t}\widehat{\mathbf{H}}_1^{\text{T}}\left(\widehat{\mathbf{H}}_1^{\text{T}}\right)^{\text{H}}\mathbf{R}_2^{-1}\right)\right]. \tag{12}$$

For the single-link case, the covariance matrix $\mathbf{R}_2$ was set to

$$\mathbf{R}_2 = \mathbf{I}_{N_r} \tag{13}$$

and for the dual-link case to

$$\mathbf{R}_2 = \eta\widehat{\mathbf{H}}_2^{\text{T}}\left(\widehat{\mathbf{H}}_2^{\text{T}}\right)^{\text{H}} + \mathbf{I}_{N_r}. \tag{14}$$

In the following, we analyze the relative sum rate capacity (SRC, or "capacity"), which is denoted by the ratio between the sum rate dual-link capacity $C(\widehat{\mathbf{H}}_1, \widehat{\mathbf{H}}_2) + C(\widehat{\mathbf{H}}_2, \widehat{\mathbf{H}}_1)$ and the sum rate single-link capacity $C(\widehat{\mathbf{H}}_1) + C(\widehat{\mathbf{H}}_2)$:

$$SRC = \frac{C(\widehat{\mathbf{H}}_1, \widehat{\mathbf{H}}_2) + C(\widehat{\mathbf{H}}_2, \widehat{\mathbf{H}}_1)}{C(\widehat{\mathbf{H}}_1) + C(\widehat{\mathbf{H}}_2)}. \tag{15}$$

In the description below *SRC* and "capacity" as well as *CMC* and "collinearity" will be used interchangeably to improve readability.

B. Simulation studies

The effect of the CCs on inter-link correlation and sum rate dual-link capacity was investigated by computer simulations in three different scenarios. In the first scenario, the locations of the clusters were changed in a controlled manner in order to study the relationships between S_{common}, *CMC* and *SRC* and the influence of the environment through a simple example. In the simulations of these *controlled channels* the environment consisted of one UCC (per link) and one CC (shared by the different links). Next, the simulation studies were continued by placing the clusters in random locations. First, the *random channels* consisted of one UCC and one CC, and, after that, of five UCCs and one CC, all being randomly positioned.

In each of the three scenarios, one MS and two BSs were located at fixed positions. The clusters consisted of five MPCs placed randomly within a diameter of one meter around the center point of the cluster. Furthermore, a 4-element x-oriented uniform linear antenna array (ULA) was used at the MS and BSs in each case. The ρ and η were both fixed to 10 dB in all the simulations. In the following, the presented *CMC* and *SRC* values are the average values over 100 independent channel realizations. Table 1 summarizes the three different simulation scenarios.

As a general conclusion of the simulation studies, it can be said that S_{common} has a significant effect on both the inter-link correlation and MIMO channel capacity; as S_{common} increases, the *CMC* increases and *SRC* decreases. This indicates the ability of the multi-link GSCM based on CCs to manipulate the correlation between different links. It also shows that it is important not to neglect the effect of common clusters.

Next, the findings from the simulation studies are discussed in detail separately for the controlled and random scenarios.

TABLE 1
SUMMARY OF THE SIMULATION SCENARIOS

Simulation scenario	Controlled	Random #1	Random #2
# BSs/MSs	2/1	2/1	2/1
# UCCs (per link)/ CCs	1/1	1/1	5/1
SNR/INR [dB]	10/10	10/10	10/10
Antenna array	4-element x-oriented ULA	4-element x-oriented ULA	4-element x-oriented ULA

1) Controlled channels

In the controlled scenario, clusters were located so that the CC and the UCC for the link MS – BS2 (UCC2) were at fixed positions whereas the UCC for the link MS – BS1 (UCC1) was moved on a circle with 45 degree steps around the MS, as shown in Fig. 2(a). The simulations with the different locations of UCC1 are marked with numbers 0 – 7 in Fig. 2a). At each location of the UCC1, the *CMC* and *SRC* were simulated with S_{common} ranging between 0 % and 100 %.

Figs. 2b) and c) show the collinearity and capacity as a function of S_{common} for the different locations of the UCC1. It is seen that the capacity is very high at low values of S_{common} in most of the locations of the UCC1, and gradually decreases to approximately 10 % of its original value as S_{common} approaches 100 %. The collinearity behaves in the opposite way, i.e. whenever the capacity is high, the collinearity is low, and vice versa. However, at UCC1 locations 3 and 5 the capacity is low, and the collinearity almost one, with all values of S_{common}. At UCC1 location 5, both UCCs are located exactly at the same position, meaning that the situation is equivalent to the case where all the clusters are common among the different links. At UCC1 location 3, there is a high correlation between the different links since the MS cannot distinguish the waves coming from locations 3 and 5 due to its antenna array orientation.

2) Random channels

As shown above, the locations of the clusters may have a significant impact on the correlation and capacity values observed at different values of S_{common}. In particular, it can be observed that with some combinations of the cluster locations collinearity is high and capacity is low even without the CC. In order to investigate the relationships between S_{common}, collinearity, capacity, and cluster locations in a statistical manner, the simulation studies were continued by placing the clusters in random locations.

The CDFs of the collinearity and capacity are shown for the first random scenario (one UCC, one CC) for the S_{common} values of 0, 1, 10, 50, 90, 99, and 100 % in Fig. 3(a) and (b). For each value of S_{common}, the CDF curve includes the values of the collinearity and capacity from 1000 random channels. With the S_{common} values of 0, 1, and 10 %, the matrix collinearity behaves quite similarly and is less than 0.2 in approximately 60 % of the cases. Even if for the most of the time the collinearity is low and capacity high with low values of S_{common}, also highly correlated channels are observed: the collinearity is at least 0.8 in about 15 % of the cases even without the CC. With the S_{common} values of 0, 1, and 10 %,

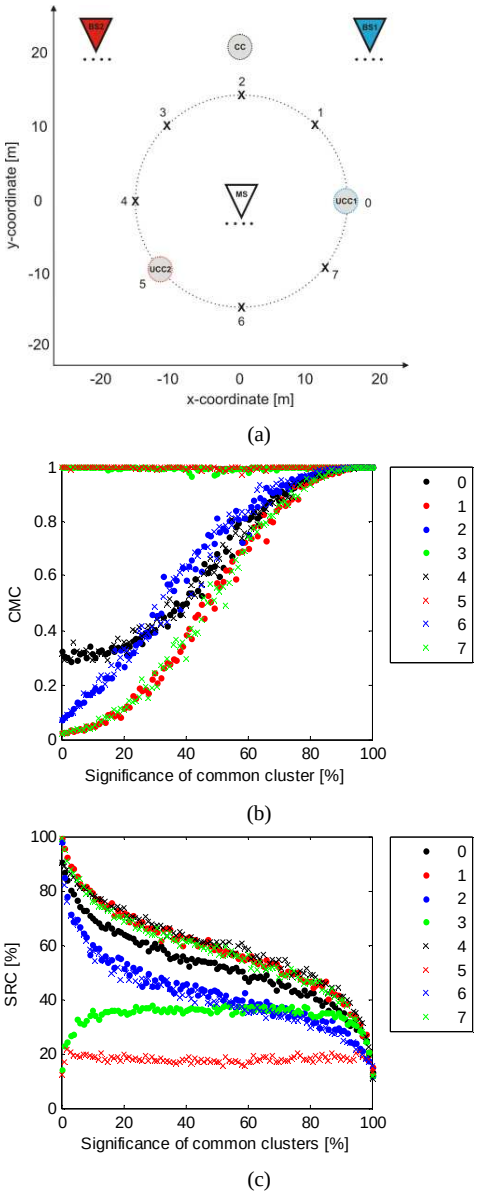

Fig. 2. Effect of common cluster simulated in controlled channels. (a) Simulation environment. (b) The correlation matrix collinearity (*CMC*), and (c) the relative sum rate capacity (*SRC*) as a function of the significance of common cluster. The legends show the correspondence between the curves and the locations of UCC1.

the capacity gets high values for the most of time, as could be expected. It was also found that that capacity is more sensitive than the collinearity to the change of S_{common} in the range of 0 to 10 %: for instance, at the CDF level of 0.5, the capacity decreased by approximately 25 %-units when S_{common} increased from 0 to 10 %. This is an important observation in the sense that even if only a small amount of the power propagates through the common cluster, the impact on the system performance is significant compared to the case where common cluster is not considered at all.

When S_{common} is 50 %, both the collinearity and capacity are almost uniformly distributed between the minimum and maximum values. With the S_{common} values of 90, 99, and 100 %, we can see that the collinearity is very close to 1 the whole time. However, variations between the respective capacity curves are more clearly seen.

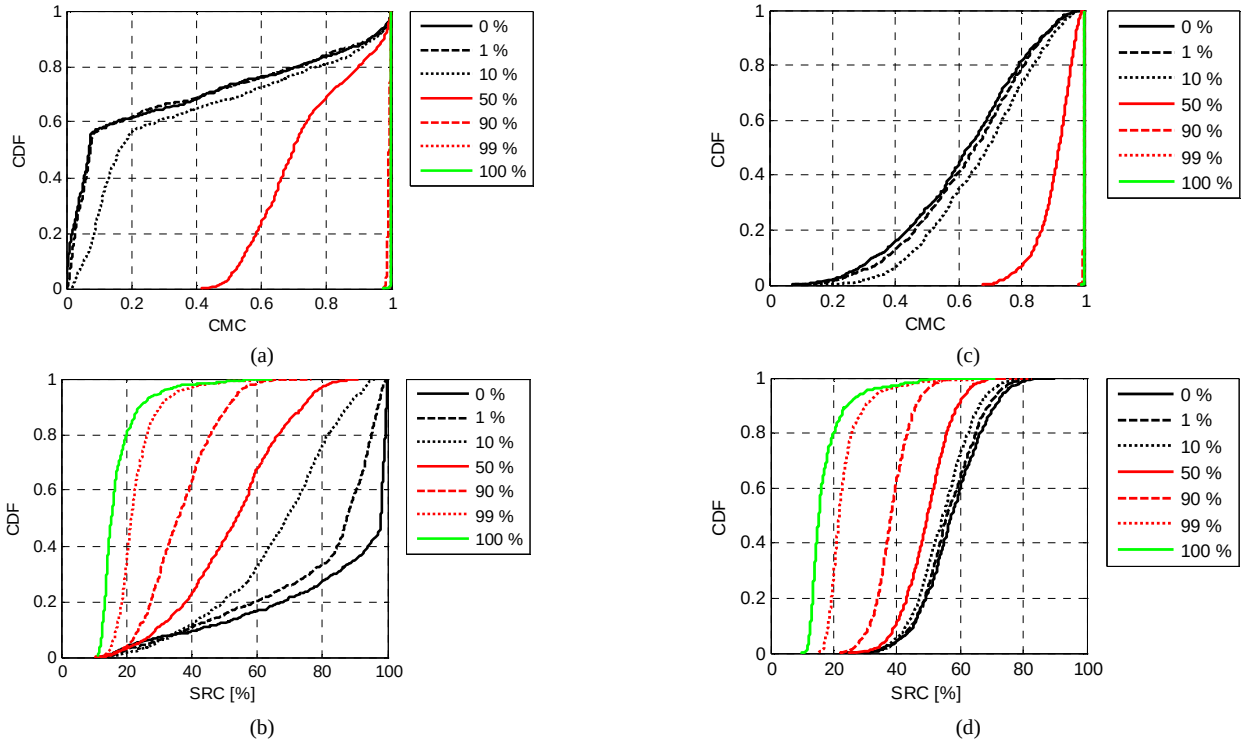

Fig. 3. Effect of common cluster on collinearity and capacity simulated in the random scenarios. CDFs of the (a) collinearity and (b) capacity in the first random scenario (one UCC, one CC). (c) Collinearity and (d) capacity in the second random scenario (five UCCs, one CC). The CDFs include data from 1000 random combinations of cluster locations with each value of the S_{common}.

The CDFs of the collinearity and capacity are shown for the second random scenario (5 UCCs, 1 CC) for the S_{common} values of 0, 1, 10, 50, 90, 99, and 100 % in Fig. 3(c) and (d). Again, the CDF curves include the values of the collinearity and capacity from 1000 random channels for each value of S_{common}.

In comparison with the first random scenario (1 UCC, 1 CC), the following observations can be made. First, with low values of S_{common} (0, 1, and 10 %), the collinearity is generally higher and therefore capacity lower; the same trends occur when S_{common} is 50 %. This can be explained so that as the number of clusters increases, it is harder for the antenna array at the MS to separate them, and hence, the correlation between links is likely to increase. Obviously, with larger antenna arrays, this effect would be less significant due to better capability of spatial filtering. With high values of S_{common} (90, 99, and 100 %), the curves are very similar to the first random scrnario, as could be expected, since anyway almost all the power propagates through the common cluster.

IV. Common Clusters in Measured Channels

Having confirmed the impact of the common clusters on the inter-link correlation and sum rate capacity, it is important to investigate how frequently the common clusters occur in real multi-link propagation scenarios. To this end, we investigate CCs based on dual-link channel measurements done in an office corridor environment. First, the methodology to extract CCs from measurement data is presented after which experimental results on S_{common} will be provided. Finally, a comparison between the measurement data and computer simulations presented in the previous section are made in terms of the sum rate capacity.

A. Extraction of common clusters from measurement data

1) Data analysis

Physical scattering objects can be identified from the measurement data by combining the measured radio propagation path parameter estimates with the geometry information of a measurement environment. In this work, the parameter estimates have been obtained by the Extended Kalman Filter (EKF) [14]. Each MPC of the EKF parameter estimates includes the DoD, DoA, delay, and polarimetric path weights. Furthermore, each propagation path obtained by the EKF has a lifetime over a certain number of consecutive measurement samples, i.e. snapshots.

In order to identify the physical scatterers for each MPC, the EKF estimates of the DoD, DoA and delay are used as inputs for a measurement-based ray tracer [15]. This ray tracer implements an algorithm that plots rays on top of a floor plan of the environment according to the measured parameter estimates. It enables the MPCs to be explicitly mapped to physical scatterers in the environment. The identification of the scattering objects can be performed simultaneously for multiple links, making it possible to study if the same physical scatterer is common for the different links, and thus forms CC.

2) Definition of a common cluster

In situations where the scatterer has a relatively large physical size, it is not always meaningful to consider the whole scatterer as common for different links. In such cases, even if the scattering source is the same physical object (e.g. a wall), the scattering points for different links might be separated by a large distance, and thereby an MS or BS equipped with antenna arrays may be able to resolve the scattering points in the angular domain. On the other hand, scattering points for the different links can be resolvable even

if the distance between them is small in a case where the scattering object is very close to the antenna. Therefore, it is necessary to establish conditions defining CCs based on 1) the distance between the scatterers of different links d, and 2) the angular separation of the scatterers seen from the MS φ, as shown in Fig. 4.

It should be noted that multiple MPCs might be originating from the same physical scatterer at the same time instant thus forming a cluster. In such cases, the distance between the scatterers of the different links is calculated based on the cluster center; the coordinates of the cluster center are calculated as the power-weighted mean over the coordinates of the scattering points of the individual MPCs belonging to the same cluster. In Fig. 4, the small black dots correspond to the scattering points of individual MPCs and the blue and red dots are the cluster centers in different links. In this work, threshold values for the d and φ are selected to be 5 meters and 45 degrees, respectively.

As stated already in Section III, the significance of common cluster(S_{common}) quantifies the amount of power that propagates through the CC. The S_{common} is determined from the measurement data in the following way. In a dual-link case, the significance of the n-th CC is denoted as a function of a measurement time instant k by

$$S^{n}_{\text{common}}(k) = \sqrt{s^{(1),n}_{\text{common}}(k) \cdot s^{(2),n}_{\text{common}}(k)}\,, \tag{15}$$

where $s^{(i),n}_{\text{common}}(k)$ is the significance of the n-th common scatterer with respect to the total power of the i-th link as

$$s^{(i),n}_{\text{common}}(k) = \frac{P^{(i),n}_{\text{common}}(k)}{P^{(i)}_{\text{tot}}(k)}\,, \tag{16}$$

where $i = 1, 2$. If the total number of scatterers that are common for the different links is denoted by $N(k)$, the total S_{common} can be expressed by the sum of the significances of the individual CCs by

$$S_{\text{common}}\,(k) = \sum_{n=1}^{N(k)} S^{n}_{\text{common}}(k)\,. \tag{17}$$

B. Significance of common clusters in an office corridor scenario

1) Measurement setup

The analyzed measurement was carried out in the corridor of the Department of Radio Science and Engineering in Aalto University by using a dual-link channel sounding system consisting of two channel sounders from Aalto University School of Science and Technology (Aalto) and Lund University (LU) operating at the frequency of 5.3 GHz [16]. The system is capable of simultaneously measuring two links having the MIMO matrix sizes of 30 × 30 and 30 × 32. A sample of a full MIMO matrix, i.e. snapshot, is measured every 39.32 ms, enabling measurements in dynamic environments. The measurement involved dual-polarization, but in the present analysis the polarizations have not been treated separately but summed up. In the measurement, the TX

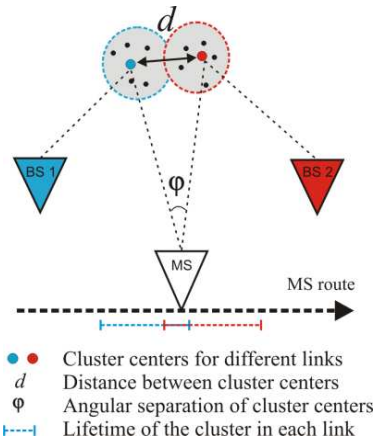

Fig. 4. Extraction of common cluster from measurement data. (a) A flow chart of the procedure for the extraction of common clusters from measurement data. (b) The distance between the scattering points of different links and the angular separation of the scattering points seen from the MS determine if the cluster is considered as common.

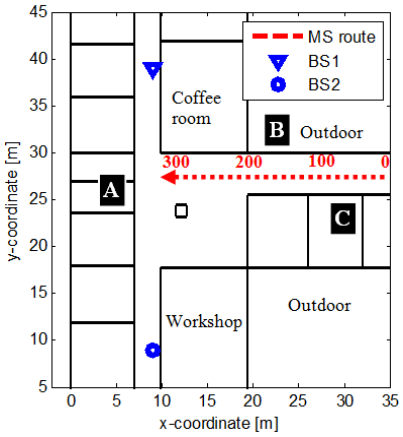

Fig. 5. The floor plan of the measurement environment in the considered scenario.

(from LU) was moved along a continuous route acting as a MS, such as a smart phone, whereas the two RXs (from LU and Aalto) were located at fixed positions to emulate WLAN BSs of neighboring cells. The floor plan of the measurement venue is shown in Fig. 5.

2) Results

The main propagation mechanism in the considered scenario is the waveguiding along the corridors in both links. In addition, DoDs pointing towards walls B and C are commonly seen on the MS side in both links. Interestingly, a noticeable share of energy propagates directly through wall B and the coffee room in the MS – BS1 link; this is possible since wall B and the right wall in the coffee room are outdoor walls having many windows meaning that the signal can penetrate the building through windows or window frames.

In order to investigate S_{common} in this scenario, the first scattering point seen from the MS on wall A was calculated and used to check the conditions for the CC. In addition, the points on wall B where the signal either propagates through the wall (MS – BS1 link) or reflects from it (MS – BS2 link) can be identified. In this scenario, other scatterers did not fulfill the criteria of the CC.

The angular separation of the scattering points on wall A and B are plotted in Fig. 6(a). In the case of wall A, the angular separation is around 10 degrees in the beginning of the route, but after snapshot 200 it starts to increase; in this location the MS passes the corner of wall C and the scattering points in the MS – BS2 link start to move further south. The threshold value is exceeded approximately at snapshot 220. In the case of wall B, the angular separation of the scattering points varies more rapidly than in the case of wall A. Furthermore, wall B is an active common scatterer only in parts of the route. The distance between the scattering points on both walls A and B (Fig. 6(b)) follow the same trends as the angular separation. Also in this case, the threshold value is exceeded in the end of the measurement route.

Fig. 7(a) shows S_{common} separately for scatterers A (blue curve) and B (red curve) and the total S_{common} (black curve). It is seen that the waveguiding along the corridor (A) is a significant propagation mechanism in both links, hence constituting a significant CC. Also wall B forms a CC in parts of the route. The total S_{common} varies between 40 % and 95 %, but goes rapidly to zero around snapshot 220 due to the fact that the threshold values for the conditions of CC are exceeded.

Fig. 7(b) shows the collinearity and capacity along the measurement route. The collinearity and capacity were calculated by applying the measured propagation path parameters obtained by the EKF to Equations (5) – (15) and by using the same 4-element linear array as in the simulations of Section III. Again, the collinearity and capacity were calculated as the mean over 100 independent realizations of the measured channels at each snapshot. Fig. 7(b) shows that the collinearity gets very high values in the beginning of the route but falls down to approximately 0.3 in the end of the route. The capacity behaves the opposite way, as was the case also in the simulation studies in Section III.

By comparing Figs. 7(a) and (b), we can clearly see that also in the measured channels, the inter-link correlation and sum rate capacity are strongly related to the significance of common clusters.

C. Comparison between measurements and simulations

Finally, in order to investigate the validity of the multi-link GSCM approach proposed in this paper, the simulations were compared with the measurements in terms of capacity.

Two measurement locations were selected for the comparison. The first location was at snapshot 120, where the S_{common} was as high as 85 %, and the second at snapshot 270, where CCs did not exist anymore. In the simulation, two UCCs (per link) and two CCs were randomly located around the simulation environment, whereas the BSs and the MS were at fixed positions.

Fig. 8 shows the CDFs of the capacity over 100 channel realizations for the measurement (solid lines) and for three independent simulation runs (dashed and dotted lines). It is seen that the simulation can always predict the dual-link channel behavior very accurately in terms of the capacity when S_{common} is 85 %. When S_{common} is 0 %, the model predicts the behavior well for the most of the time; however, occasionally, due to random cluster locations, the correlation between links happens to be high in the simulation which results in underestimation of the capacity.

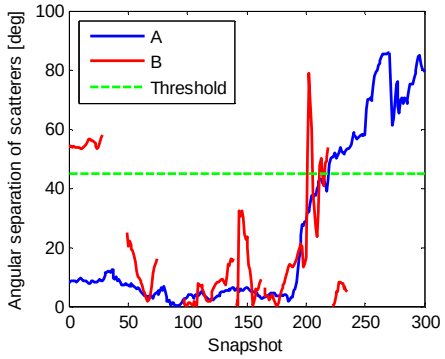

(a)

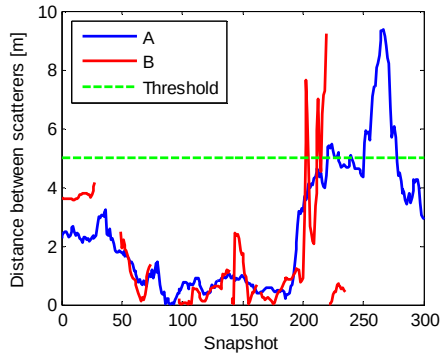

(b)

Fig. 6. (a) The angular separation of the scattering points belonging to the different links seen from the MS. (c) The distance between the scattering points of different links.

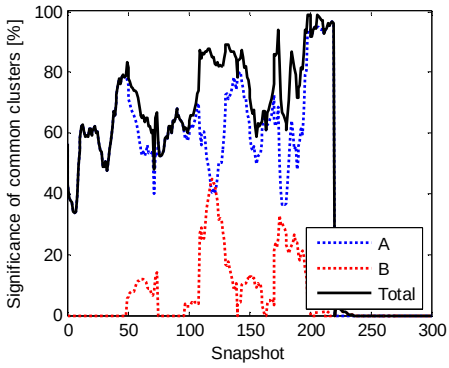

(a)

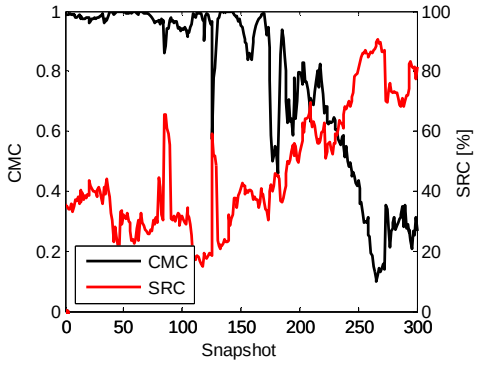

(b)

Fig. 7. (a) The significance of common clusters and (b) collinearity (black curve) and capacity (red curve) as a function of the measurement location in snapshots.

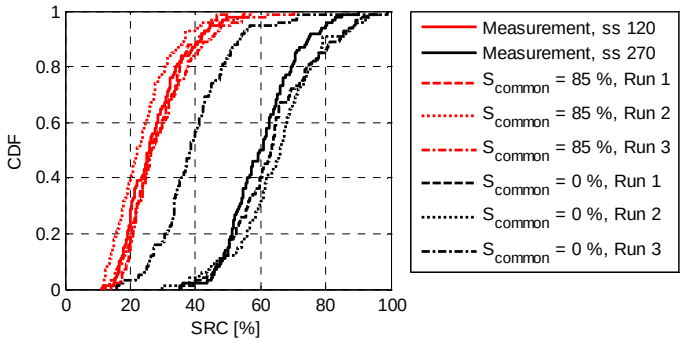

Fig. 8. Comparison between measurements and simulations. The CDFs of the capacity at snapshots 120 and 270 and of three independent simulation runs with corresponding significance of common cluster are shown. In the simulations, 2 UCCs (per link) and 2 CCs were generated in random locations.

V. Conclusion

In this paper, an approach to extend geometry-based stochastic channel models (GSCMs) to support multi-link simulations has been presented. The proposed approach is based on the concept of *common clusters (*CCs): the correlation between different MIMO links, i.e. the inter-link correlation, is controlled by adjusting the amount of power that simultaneously propagates via the same clusters in the different links. A multi-link GSCM was implemented, and the effects that the CCs have on inter-link correlation and on sum rate capacity were investigated based on simulations. The existence of CCs in real-world channels was confirmed by dual-link channel measurements in an office corridor scenario. The measurement results revealed that the significance of CCs can be as high as 95 %.

In both simulations and measurements, clear relations were found between the CC power, the inter-link correlation, and the sum rate dual-link capacity. Generally, as the amount of power carried by the CCs increases, the inter-link correlation increases and at the same time the sum rate capacity decreases. In addition, comparison between simulations and measurements in terms of the sum rate dual-link capacity revealed good agreement, indicating the validity of the proposed multi-link GSCM.

The results of the paper indicate that the developed CC-based multi-link GSCM provides a suitable means for controlling the correlation between different MIMO links in a realistic manner. Furthermore, it is evidently vital to include CCs in GSCMs since neglecting them would lead to too optimistic performance results in system simulations.

Acknowledgments

The authors would like to thank Dr. Peter Almers, Dr. Traian Abrudan, Dr. Andreas Richter, and Mr. Jukka Koivunen for their help in measurements and data processing. Dr. Jussi Salmi is acknowledged for providing the codes for calculating the parameter estimates; and Mr. Alvaro Palacios for his help in developing the channel model implementation.

References

[1] A. F. Molisch, H. Asplund, R. Heddergott, M. Steinbauer, and T. Zwick, “The COST 259 directional channel model – part I: overview and methodology,” *IEEE Transactions on Wireless Communications*, vol. 5, no. 12, December 2006.

[2] Luis M. Correia (ed.), Mobile Broadband Multimedia Networks – Techniques, Models and Tools for 4G, Elsevier, Oxford, UK, 2006, 569p.

[3] WINNER II deliverable D1.1.2 V1.1, *WINNER Channel Models.* Online: http://www.ist-winner.org/deliverables.html.

[4] F. Kaltenberger, D. Gesbert, R. Knopp, and M. Kontouris, ”Correlation and capacity of measured multi-user MIMO channels,” in *Proc. IEEE 19th International Symposium on Personal, Indoor and Mobile Radio Communications (PIMRC 2008)*, pp. 1 – 5, Cannes, France, September 2008.

[5] J. Poutanen, K. Haneda, J. Salmi, V.-M. Kolmonen, and P. Vainikainen, “Analysis of correlated shadow fading in dual-link indoor radio wave propagation,” *IEEE Antennas and Wireless Propagation Letters*, vol. 8, pp. 1190 – 1193, 2009.

[6] J. Poutanen, K. Haneda, J. Salmi, V.-M. Kolmonen, T. Hult, F. Tufvesson, and P. Vainikainen, “Significance of common scatterers in multi-link radio wave propagation,” in *Proc. 4th European Conference on Antennas and Propagation 2010 (EuCAP 2010)*, p1849081, Barcelona, Spain, April, 2010.

[7] V.-M. Kolmonen, K. Haneda, T. Hult, J. Poutanen, F. Tufvesson, and P. Vainikainen, ”Measurement-based evaluation of interlink correlation for indoor multi-user MIMO channels,” *IEEE Antennas and Wireless Propagation Letters*, vol. 9, pp. 311 – 314, 2010.

[8] V.-M. Kolmonen, K. Haneda, F. Tufvesson, J. Poutanen, and P. Vainikainen, "A dual-link capacity analysis of measured time-variant indoor channel," accepted for publication in *Electronics Letters*, 2010.

[9] N. Czink, B. Bandemer, G. Vazquez-Vilar, L. Jalloul, C. Oestges, and A. Paulraj, ”Spatial separation of multi-user MIMO channels,” in *Proc. IEEE 20th International Symposium on Personal, Indoor and Mobile Radio Communications (PIMRC 2009)*, pp. 1059 – 1063, Tokyo, Japan, September 2009.

[10] T. Hult, F. Tufvesson, V.-M. Kolmonen, J. Poutanen, and K. Haneda, ”Analytical dual-link MIMO channel model using correlated correlation matrices,” in *Proc. 4th European Conference on Antennas and Propagation 2010 (EuCAP 2010)*, p1849792, Barcelona, Spain, April, 2010.

[11] A. Molisch, M. Steinbauer, M. Toeltsch, E. Bonek, and R. Thoma, “Capacity of MIMO systems based on measured wireless channels,” *IEEE Journal on Selected Areas in Communications*, vol. 20, no. 3, pp. 561–569, Apr. 2002.

[12] G. Golub and C. van Loan, *Matrix computations*, 3rd ed. London: The Johns Hopkins University Press, 1996.

[13] R. Blum, “MIMO capacity with interference,” *IEEE Journal on Selected Areas in Communications*, vol. 21, no. 5, pp. 793 – 801, 2003.

[14] J. Salmi, A. Richter, and V. Koivunen, “Detection and tracking of MIMO propagation path parameters using state-space approach,” *IEEE Transactions on Signal Processing*, vol. 57, no. 4, pp. 1538–1550, April, 2009.

[15] J. Poutanen, K. Haneda, J. Salmi, V-M Kolmonen, A. Richter, P. Almers, and P. Vainikainen, “Development of measurement-based ray tracer for multi-link double directional propagation parameters,” in *Proc. 3rd European Conference on Antennas and Propagation 2009 (EuCAP 2009)*, pp. 2622–2626, Berlin, Germany, Mar., 2009.

[16] V.-M. Kolmonen, P. Almers, J. Salmi, J. Koivunen, K. Haneda, A. Richter, F. Tufvesson, A. F. Molisch, and P. Vainikainen, “A dynamic dual-link wideband MIMO measurement system for 5.3 GHz,” *IEEE Transactions on Instrumentation and Measurement*, vol. 59, no. 4, pp. 873 – 883, March 2010.